Bioorg. Med. Chem. Lett. 47 (2021) 128209

Contents lists available at ScienceDirect

Bioorganic & Medicinal Chemistry Letters

journal homepage: www.elsevier.com/locate/bmcl

Discovery of quinuclidine modulators of cellular progranulin

James C. Lanter *, Angela Y.-P. Chen, Toni Williamson, Gerhard Koenig, Jean-François Blain, Duane A. Burnett

Arkuda Therapeutics, 200 Arsenal Yards Blvd Suite 220, Watertown, MA 02472, USA

ARTICLE INFO

Keywords:
Progranulin
Frontotemporal dementia
Quinuclidine
Neurodegeneration
CNS

ABSTRACT

Phenotypic screening of an annotated small molecule library identified the quinuclidine tetrahydroisoquinoline solifenacin (**1**) as a robust enhancer of progranulin secretion with single digit micromolar potency in a murine microglial (BV-2) cell line. Subsequent SAR development led to the identification of **29** with a 38-fold decrease in muscarinic receptor antagonist activity and a 10-fold improvement in BV-2 potency.

Frontotemporal dementia (FTD) is the second most common form of dementia after Alzheimer's disease (AD), but, compared to AD, FTD is considered a rare disease with an incidence estimated to be 1.6–4.1/100,000 annually.[1–3] This disorder is distinguished by its age of onset, rate of progression and localization in the frontal and temporal lobes, impacting personality, behavior, language, memory and movement. FTD of the progranulin subtype (FTD-*GRN)* represents about 25% of cases,[4] and is caused by autosomal dominant mutations[5] in the gene encoding the secreted glycoprotein progranulin (PGRN). All known mutations cause haploinsufficiency leading to reduced levels of PGRN, suggesting that its restoration to normal levels will be therapeutically beneficial to such patients. The current absence of an effective treatment makes at-risk subjects often choose not to be genotyped possibly also contributing to an underestimation of the patient population. This point highlights the urgent need for therapies that will not only affect the course of the disease, but also prevent, or at least delay, the onset of behavioral symptoms and cognitive decline.

It is in this context that we initiated a program to identify small molecules effective in raising PGRN levels. To this end we employed a phenotypic screening approach utilizing an immortalized murine microglial line (BV-2) to evaluate a moderately sized chemogenomic[6] library of about 3500 molecules.[7] The members of this library were chosen with annotated activity across a range of molecular targets spanning all major protein classes: G-protein coupled and nuclear receptors, enzymes, transporters, and ion channels. To date, small molecule enhancers of PGRN release have only demonstrated effectiveness in preclinical models. Conversely an anti-sortilin monoclonal antibody was shown raise CSF PGRN in the clinic, albeit by blocking a major avenue of PGRN cellular entry. Of the small molecules, lysosome alkalizing agents (Bafilomycin A and chloroquine),[8] histone deacetylase inhibitors as well as mTOR inhibitors and the autophagy activator trehalose[9] have been reported to induce PGRN secretion. Several molecules representing these mechanisms were part of the library and served as positive controls in the initial screen. Among the molecules screened, one stood out from the others: the muscarinic receptor antagonist drug solifenacin[10] (Fig. 1, **1**). Two features of this hit raised its profile: muscarinic receptor antagonism was not reported in the literature to affect progranulin levels and evaluation of the scaffold using a multiparameter optimization algorithm[11] for CNS drug like properties indicated that it had good potential for brain distribution relative to the periphery.

It was encouraging to see that our first modification, reversal of the quinuclidine configuration (Fig. 1, **2**), maintained the BV-2 potency while reducing the annotated (M3 antagonist) activity more than 30-fold, suggesting that muscarinic receptor engagement was not involved in progranulin release. With this information, we began our SAR development by exploring substitution on the phenyl substituent pendant to the tetrahydroisoquinoline (THIQ) ring. To enable this and subsequent SAR work we employed the synthetic route depicted in Scheme 1. Acylation of phenethylamine followed by Bischler-Napieralski[12] cyclization delivered the right half architecture. Reduction of the cyclic imine was accomplished via hydrogenation with concomitant creation of a stereocenter at the 1-position of the bicycle. For SAR exploration of the pendant aryl ring, resolution of the antipodes was effected by chiral chromatography but for exploring the SAR of analogs with a fixed aryl moiety, iridium catalyzed asymmetric hydrogenation[13] was employed to provide optically pure material. Coupling of this material to the quinuclidine was typically done by activating the latter as even carbamoyl chlorides of the THIQ were of generally low reactivity.

* Corresponding author.

https://doi.org/10.1016/j.bmcl.2021.128209
Received 1 April 2021; Received in revised form 10 June 2021; Accepted 14 June 2021
Available online 18 June 2021

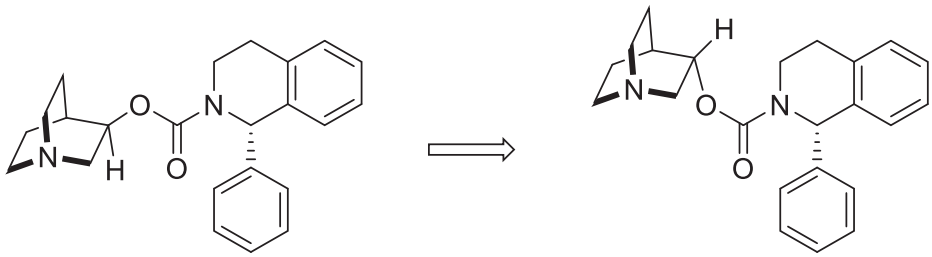

Solifenacin, **1**
BV-2 EC_{50}: 1300 nM
M3 Ant EC_{50}: 24 nM

2
BV-2 EC_{50}: 1800 nM
M3 Ant IC_{50}: 730 nM

Fig. 1. Screening hit and initial analog.

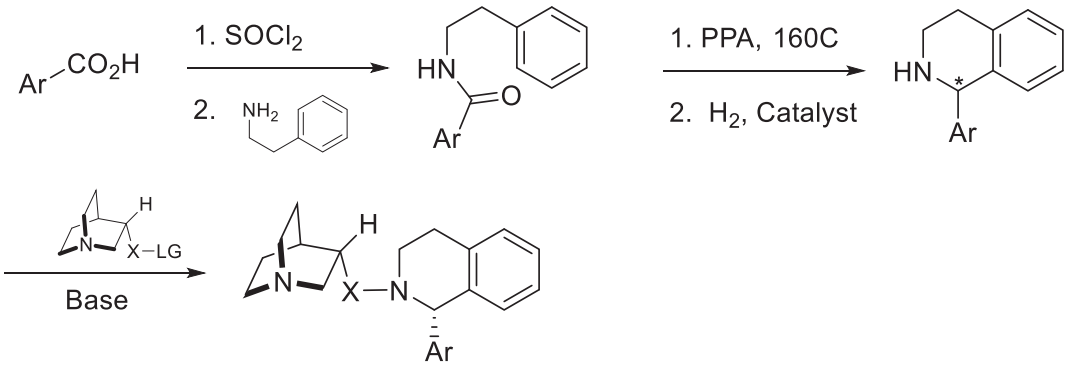

Scheme 1. Synthesis of Quinuclidine THIQ.molecules.

Table 1
Pendant aryl ring SAR.

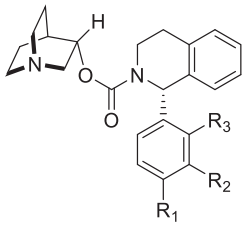

Compound	R_1	R_2	R_3	PGRN EC_{50}[a]	M3 IC_{50}[b]
1				1300	24
2	H	H	H	1830	733
3	F	H	H	257 ± 138	17,000
4	Cl	H	H	339 ± 33	1480
5	OMe	H	H	2870	–
6	OCF_3	H	H	2600	–
7	O*cyc*Pr	H	H	>10,000	–
8	SO_2Me	H	H	>10,000	–
9	H	F	H	3550	
10	F	F	H	2030	10,000
11	F	H	F	247 ± 138	9400
12	H	F	F	1110	

[a] in BV-2 cells (nM, ±SD; Values are the average of duplicate runs. Where reported, standard deviation values are calculated from multiple assays).
[b] (nM).

Table 2
Linker SAR.

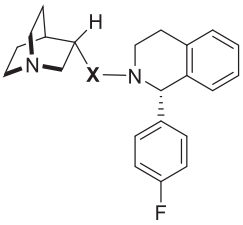

Compound	X	PGRN EC_{50}[a]	M3 IC_{50}[b]	MPO Score
3	–OCO-	257 ± 138	17,000	4.19
13	–NHCO-	265 ± 133	10,000	4.92
14	-NMeCO-	1030 ± 253	–	4.34
15	$–CH_2CO-$	222 ± 38	30,000	4.17
16	$–OCH_2CO-$	811	–	4.92
17	–CH(OH)CO–	895	–	5.28
18	$-CH_2SO_2-$	1700	–	5.35
19	$-NHSO_2-$	>10000	–	5.17
20	–NHCOCO-	1610	–	5.24
21	–OCOCO-	>10000	–	4.50
22	$–CH_2CH(CF_3)-$	3070	–	1.96

[a] in BV-2 cells (nM, ±SD; Values are the average of duplicate runs. Where reported, standard deviation values are calculated from multiple assays).
[b] (nM).

While most quinuclidine derivatives were commercially available, in select cases (e.g. **15**) quinuclidine-3-one was a useful precursor.

Representative results of a comprehensive SAR survey of the pendant aryl ring revealed a narrow tolerance for substitution (Table 1). Addition of a fluorine atom to the 4-position (**3**) led to both a profound reduction in muscarinic receptor activity as well as a substantial increase in BV-2 potency.

Surprisingly, while installing a chlorine (**4**) at the same position maintained the BV-2 potency, it also increased the M3 activity 10-fold. Further exploration of 4-position substituents with either electron donating (**5**, **7**) or withdrawing (**6**, **8**) substituents led to a substantial

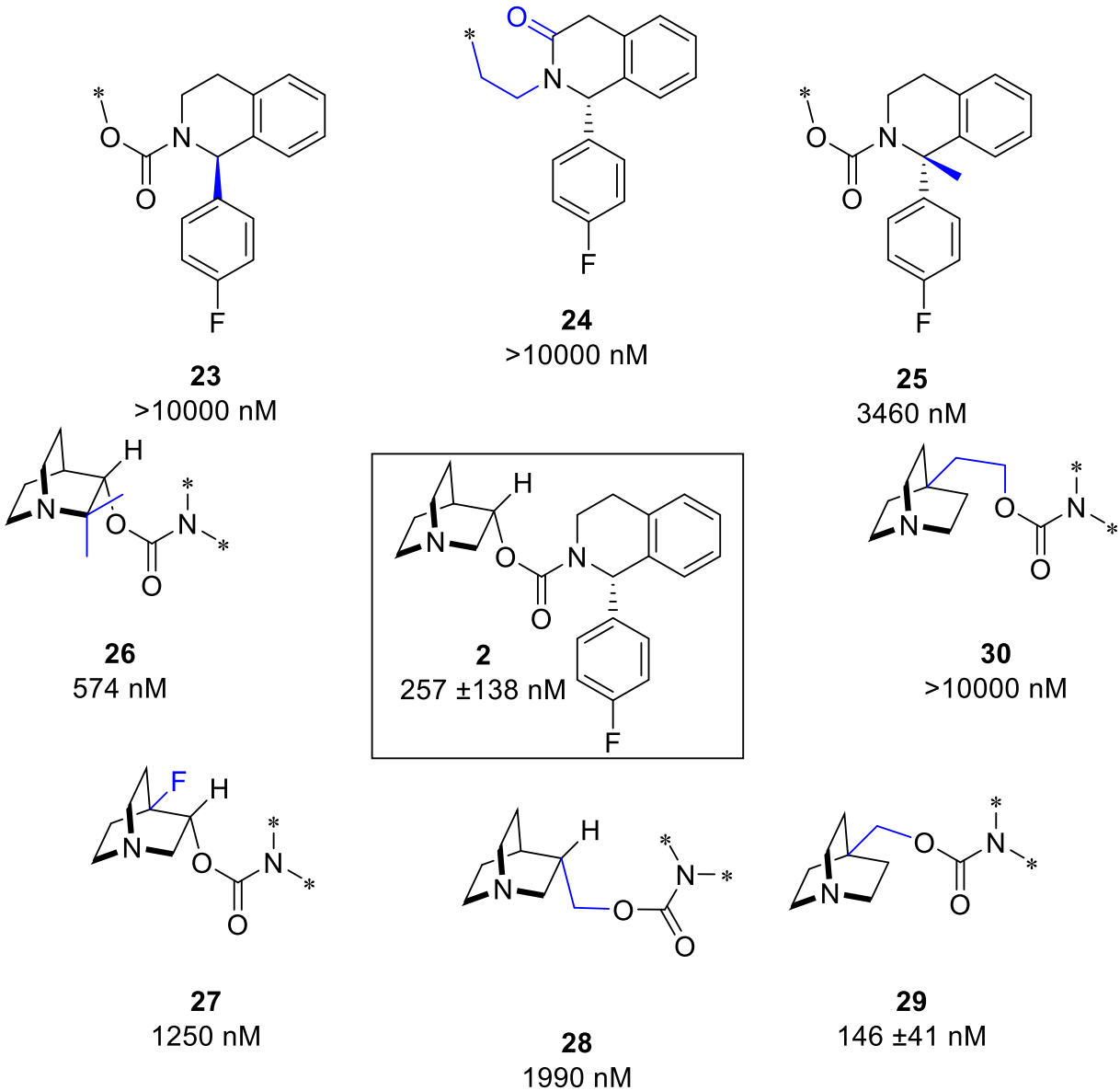

Fig. 2. Further SAR exploration; asterisks indicate unchanged portions of structure **2**(PGRN EC_{50} in BV-2 Cells[a]). [a] in BV-2 cells (nM, ±SD; Values are the average of duplicate runs. Where reported, standard deviation values are calculated from multiple assays).

decrease in potency. These results prompted us to look in greater detail at fluorine substitution. Moving the atom from the 4- to the 3-position (**9**) caused about a 10-fold drop in potency as did adding a fluorine atom to the 3-position (**10**) of **3**. While the 2,4-difluoro analog (**11**) maintained BV-2 potency on par with **3**, the 2,3-difluoro molecule (**12**) was about 4-fold less potent. A wide variety of polar substituents, heteroatom substitutions and fused heterocycles on the pendant ring, as well as a smaller group of conservative modifications on the fused aromatic ring were also explored (data not shown). None of these analogs were more active than those reported in Table 1, indicating **3** represented an optimized right hemisphere of the pharmacophore.

We next turned our attention to the linker between the right hemisphere and the quinuclidine, selecting a conservative group of alternatives with good, predicted properties (Table 2). Compared to the carbamate (**3**), both the trisubstituted urea (**13**) and the amide (**15**) maintained not only the high level of cellular potency but also a good margin with M3 receptor engagement. None of the other linkers assessed (**16**–**21**) including the *N*-methyl substituted urea (**14**) were able to maintain enough of the cellular potency to warrant further investigation. Bioisosteric replacement of the amide linker (**22**) with trifluoroethyl amine,[14] in addition to losing more than ten-fold BV-2 potency (as a 1:1 diastereomeric mixture), also suffered from a reduced MPO score and was not further pursued.

Having established the quinuclidine stereochemistry needed to mitigate muscarinic receptor engagement, optimized pendant aryl ring substitution and explored a range of linkers to connect the two halves of the molecule, we turned our attention to both the tetrahydroisoquinoline and quinuclidine moieties. Although the SAR shown thus far incorporates (*S*) stereochemistry off the THIQ ring, as a consequence of our synthetic approach the (*R*) isomers of most compounds were also isolated and tested. Without exception, they were less potent than the (S) configured molecules as exemplified by compound **23** vs **2** (Fig. 2,). Moving the carbonyl from the linker (**15**) to the THIQ ring (**24** vs **15**) was also deleterious to the activity as were other changes to the scaffold such as installation of a methyl group next to the pendant fluorophenyl ring (**25**). Steric shielding of the quinuclidine basic nitrogen (**26**), quinuclidine fluorination (**27**) or homologation of the linker (**28**) all reduced potency to varying degrees. Interestingly, moving the

Table 3
In vitro ADME properties for selected molecules.

Compound	MDCK-MDR1[a] $P_{appA\rightarrow B}$ [ER]	Aqueous Solubility[b]	Protein Binding[c], F_u	Brain Tissue Binding[c], F_u	Hepatocytes $t_{1/2}$[d], CL_{int}[e]
3	7.59 [0.94]	1990	2.0 (m) 8.6 (r) 6.0 (h)	0.8 (m) 0.8 (r)	29, 23.0(r) 10, 69.8 (c) >240, 1.9 (h)
13	0.95 [39.46]	5965	–	–	–
15	2.68 [18.90]	–	–	–	–
29	3.01 [3.62]	2670	4.8 (m) 9.6 (r) 17.6 (c) 8.6 (h)	0.8 (m) 0.7 (r)	17, 39.7 (r) 22, 31.8(c) 198, 3.5(h)

[a] (*10^{-6} cm/s).
[b] μM, pH 7.4 (PBS).
[c] %; m: mouse, r: rat, d: dog; c: cynolmologous monkey, h: human.
[d] minutes.
[e] μL/min/kg.

Table 4
Pharmacokinetic parameters for **3** and **29**.

Compound (Species)	Dose IV/PO	PO $t_{1/2}$ (h)	IV $t_{1/2}$ (h)	$C_{max,u}$ (nM)	K_{puu} @ 8 h	F (%)	CL[a]	V_{dss}[b]
3 (mouse)	1/10	4.1	2.1	28	1.08	64	2.65	4.91
3 (rat)	1/10	2.1	1.9	37	0.26	16	11.9	4.65
29 (mouse)	1/10	2.9	2.2	30	0.09	41	3.11	7.23
29 (rat)	1/10	5.2	2.2	17	0.40	16	6.09	16.2
29 (cyno)	1/3	6.8	6.4	32	0.33	42	1.24	9.60

[a] L/h/kg.
[b] L/kg.

attachment point from the 3- to the 4-position of the bicyclic amine was well tolerated (**29**) though the homolog (**30**) was not. All attempts to directly connect the 4-quinuclidinol to the THIQ as a carbamate failed, likely due to an unfavorable steric environment during coupling.

With several interesting molecules in hand, we proceeded to assess their *in vitro* ADME properties (Table 3). It became immediately apparent from their poor permeability and efflux ratio (ER) that neither the urea (**13**) nor amide (**15**) linkers merited further investigation. Of the two remaining molecules, the 3-substituted quinuclidine (**3**) had superior permeability and efflux potential compared to the 4-substitued molecule (**29**) though they were similar across measures of protein binding, nonspecific brain tissue binding and intrinsic clearance.

We next evaluated the pharmacokinetic properties of both molecules in mice and rats (Table 4). While **3** outperformed **29** in mice with respect to its unbound partition coefficient (K_{puu}), other PK parameters were similar. In contrast, rat PK data indicated that **29** regained substantial ground on the K_{puu} front, albeit at some expense to oral bioavailability and clearance. The cynomologus monkey PK parameters of **29** echoed its mouse data with the notable exceptions of K_{puu} and half-life. In aggregate, both molecules have pharmacokinetic characteristics suitable for the exploration of progranulin changes *in vivo*; such work is ongoing and will be reported in due course.

In summary, cellular phenotypic screening of an annotated small molecule library delivered a tractable scaffold for further investigation. Systematic modification of this hit greatly reduced the known muscarinic receptor antagonist activity while substantially improving the potency of the desired progranulin-releasing effects. Two molecules were identified with ADME-PK properties warranting further *in vivo* investigation.

Declaration of Competing Interest

The authors declare the following financial interests/personal relationships which may be considered as potential competing interests: The authors are currently, or were at the time the work was performed, employees of Arkuda Therapeutics. A central goal of Arkuda Therapeutics is the discovery of small molecule modulators of progranulin for the treatment of Frontotemporal dementia.

Acknowledgements

The authors would like acknowledge several partners in the reported work. Andrew Cook designed the chemogenomic library from which solifenacin's progranulin releasing activity was discovered. Mark Tebbe served as a chemistry consultant in the early days of the company and William Greenlee has been a valuable medicinal chemistry resource throughout our journey. All the compounds reported were synthesized by partners at Symeres and Shanghai ChemPartner. The latter organization also conducted both *in vitro* ADME and *in vivo* DMPK characterizations.

Appendix A. Supplementary data

Supplementary data to this article can be found online at https://doi.org/10.1016/j.bmcl.2021.128209.

References

1 Woollacott IOC. *Toher JD Neurochemistry*. 2016;138:6.
2 Coyle-Gilchrist ITS, Dick KM, Patterson K, et al. *Neurology*. 2016;86(18):1736.
3 Knopman DS, Roberts RO. *J Mol Neurosci*. 2011;54(3):330.
4 Mackenzie IRA. *Acta Neuropathol*. 2007;114(1):49.
5 van Swieten JC, Heutink P. *Lancet Neurol*. 2008;10(965).
6 Jones LH, Bunnage ME. *Nat Rev Drug Discov*. 2017;16:285.
7 (a)Larson K, Cook, A, Soper, J et al. A phenotypic screen of a mouse microglial cell line reveals novel mechanisms to modulate levels of progranulin. in 9th ICFTD), Vancouver, Canada, 2014; Abstract 137.
(b)Cook A, Larson, KC, Soper, JH, et al. Building a compound phenotypic screening collection and the discovery of mechanisms to modulate levels of progranulin to treat FTLD in BSOBC, Boston, MA, 2014.
8 Capell A, Liebscher S, Fellerer K, et al. *J Neurosci*. 2011;31(5):1885.
9 Cenik B, Sephton CF, Dewey CM, et al. *J Biol Chem*. 2011;18:16101.
10 Basra R, Kelleher C. *Ther Clin Risk Manag*. 2008;4(1):117.
11 Wager TT, Hou X, Verhoest PR, et al. *ACS Chem Neurosci*. 2016;7(6):767.
12 Heravi MM, Khaghaninejad S, Nazari N. *Adv Het Chem*. 2014;112:183.
13 Kim AN, Ngamnithiporn A, Welin ER, et al. *ACS Catal*. 2020;10(5):3241.
14 Black WC, Bayly CI, Davis DE, et al. *Bioorg Med Chem Lett*. 2005;15(21):4741.